Pergamon

Cement and Concrete Research 32 (2002) 379–385

CEMENT AND CONCRETE RESEARCH

Defect dynamics of cement mortar under repeated loading, studied by electrical resistivity measurement

Jingyao Cao, D.D.L. Chung*

Composite Materials Research Laboratory, University at Buffalo, Department of Mechanical and Aerospace Engineering, The State University of New York, Buffalo, NY 14260-4400, USA

Received 20 September 2000; accepted 17 September 2001

Abstract

Defect dynamics, as studied by electrical resistivity measurement during repeated compression of cement mortar in the elastic regime, are characterized by defect generation, defect healing and defect aggravation. Defect generation dominates in the first compressive loading and in tensile loading in any loading cycle. Defect healing dominates in all subsequent compressive loading cycles and in tensile unloading in any cycle. Defect aggravation dominates during compressive unloading in any cycle and occurs during tensile loading in any cycle. Both the interface between sand and cement and that between silica fume and cement contribute to the defect dynamics, particularly the defect healing. The defect dynamics give similar effects to the longitudinal and transverse resistivities. Upon uniaxial compression, the resistivity decreases (except for the first cycle); upon uniaxial tension, the resistivity increases.

Keywords: Microcracking; Microstructure; Electrical Properties; Strain effect; Mortar

1. Introduction

Defects in a solid respond to applied stresses. When the applied stress is dynamic, the response of the defects is also dynamic. The response encompasses the generation, healing and aggravation of defects [1]. Defect generation refers to the formation of defects, which usually occurs during loading. Defect healing refers to the diminution of defects. Healing can occur during compressive loading of a brittle material, such as a cement-based material. Defect aggravation refers to the propagation or enlargement of defects; it can occur during removal of a compressive stress from a brittle material.

Previous work on defects in cement-based materials has emphasized the effects of plastic deformation and damage. Due to the irreversible nature of these processes, the observation of their effects does not require monitoring during deformation. In contrast, this work addresses the effects of elastic deformation. Due to the reversible nature of elastic deformation, the observation of the effects of elastic deformation requires monitoring in real time during deformation. Moreover, the method of monitoring must be sensitive to the subtle effects of elastic deformation on the defects. For example, modulus measurement is not sensitive to the effects of elastic deformation. Because of these difficulties, there has been little prior work on the defect dynamics during elastic deformation [1].

The characterization of defect dynamics is of both scientific and technological interest, as it relates to materials science as well as material durability and reliability. In particular, it provides an understanding of the microstructural effects of elastic deformation, which is commonly encountered by concrete structures during normal use. In contrast, plastic deformation and damage are not usually encountered during normal use. Hence, knowledge of the defect dynamics during repeated loading and unloading in the elastic regime is useful for the design and use of concrete structures.

Previous work on defect dynamics has addressed cement paste under repeated compression in the elastic regime [1]. As indicated by electrical resistivity measurement, defect generation dominates during first loading, defect healing dominates during subsequent loading, and defect aggravation dominates during subsequent unloading. This work extends the study from cement paste to mortar. Cement

* Corresponding author. Tel.: +1-716-645-2593; fax: +1-716-645-3875.
E-mail address: dlchung@acsu.buffalo.edu (D.D.L. Chung).

0008-8846/02/$ – see front matter
PII: S0008-8846(01)00686-X

paste differs from mortar in the absence of a fine aggregate. Hence, mortar has in it an interface between the aggregate and the cement paste. This interface is absent in cement paste. As this interface can be a location for defects, mortar contains some defects, which are absent in cement paste. Therefore, comparison of the defect dynamics in mortar and cement paste is of interest. Moreover, the presence of an aggregate makes mortar a step closer to concrete.

Previous work on defect dynamics has emphasized the effect of plastic deformation and its relevance to damage and failure [2–14]. In contrast, this paper is not centered on damage, but on defect dynamics under repeated loading in the elastic regime.

Additives are often used in concrete mixes in order to improve the properties. An example of an additive is silica fume (a particulate of typical size around 0.1 μm), which enhances the mechanical properties and decreases the permeability [15–33]. This work also addresses the effect of silica fume on the defect dynamics.

2. Experimental methods

The cement used was Portland cement (Type I) from Lafarge (Southfield, MI). The sand used was natural sand (100% passing 2.36-mm sieve, 99.9% SiO_2). The sand/cement ratio was 1.0. 15% by mass of cement of silica fume (Elkem Materials, Pittsburgh, PA, EMS 965) was used. Two percent by mass of cement of a water reducing agent (WR) was used. The WR was TAMOL SN (Rohm and Haas, Philadelphia, PA) that contained 93–96% sodium salt of a condensed naphthalene sulfonic acid. The water/cement ratio was 0.35. No coarse aggregate was used. A Hobart mixer with a flat beater was used for mixing. The mix was mixed for 5 min. The mix was then poured into oiled molds and a vibrator was used to facilitate compaction and reduction of air bubbles.

Two types of mortar were studied. First, plain mortar consisting of cement, sand, water and WR. Second, silica fume mortar consisting of cement, water, WR and silica fume. Six specimens of each type were tested. Unless noted otherwise, plain mortar was used.

Compressive testing was performed in accordance with ASTM C109-80, as described in Ref. [1]. Specimens were prepared using a $2 \times 2 \times 2$ in ($51 \times 51 \times 51$ mm) mold. The strain was measured by using a strain gage. Compressive testing under load control was performed using a hydraulic mechanical testing system (MTS Model 810). Testing was conducted under repeated loading (load control) and at stress amplitudes (either increasing cycle by cycle or fixed for all cycles) within the elastic regime. The time period for a stress cycle was 20 s. In the case of a fixed stress amplitude, 34.5 MPa, the loading speed was 3.45 MPa/s.

During compressive testing of the cubes mentioned above, the longitudinal resistivity was measured using the four-probe method, as described in Ref. [1]. A Keithley 2002 multimeter was used.

Rectangular bars of size $160 \times 40 \times 40$ mm were used for transverse resistivity measurement during uniaxial compression. Each electrical contact was applied around the entire 40×40 mm perimeter of the bar. The voltage (inner) contacts were placed on two parallel cross-sectional planes that were 100 mm apart. The current (outer) contacts were placed on planes that were 120 mm apart. Thus, the resistivity was measured along the length of the rectangular bar, using the four-probe method. During the resistivity measurement, compressive stress was applied to the middle portion (40×40 mm) of the rectangular specimen (Fig. 1). The electrical contacts were arranged away from the stressed portion and the stress was perpendicular to the direction of resistivity measurement. The stress (cyclicly loaded at a stress amplitude of 13.90 MPa with a loading speed of 1.39 MPa/s and a period of 20 s) was provided by a hydraulic mechanical testing system (MTS Model 810 under load control). The transverse strain was measured using a strain gage attached to the side of the specimen, as shown in Fig. 1.

Dog-bone shaped specimens of the dimensions shown in Fig. 2 were used for tensile testing. The specimen's cross-sectional area was 30×20 mm in the narrow part of the dog-bone shape. Specimens were prepared by casting into molds of the same shape and size. Tensile testing was performed using a Sintech 2/D screw-action mechanical testing system under cyclic loading (load control) at a stress magnitude of 1.48 MPa and a period of 48 s. The loading speed was 0.0617 MPa/s.

During tensile testing, both longitudinal and transverse strains were measured with strain gages attached to the

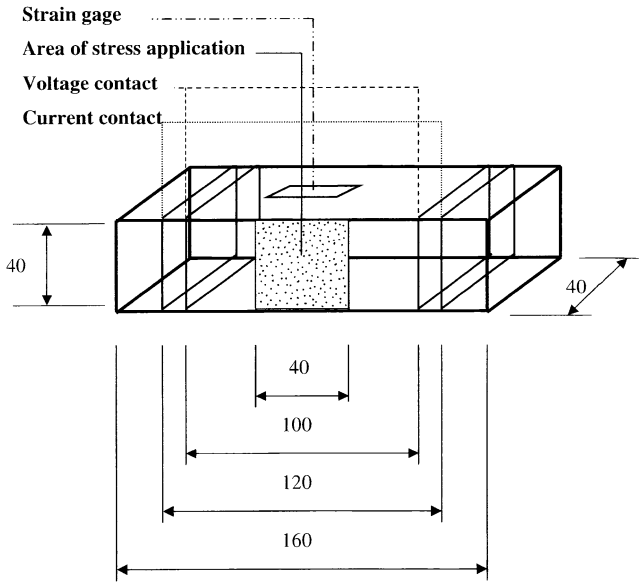

Fig. 1. Sample configuration for measuring the transverse electrical resistivity during uniaxial compression. Dimensions are in millimeters.

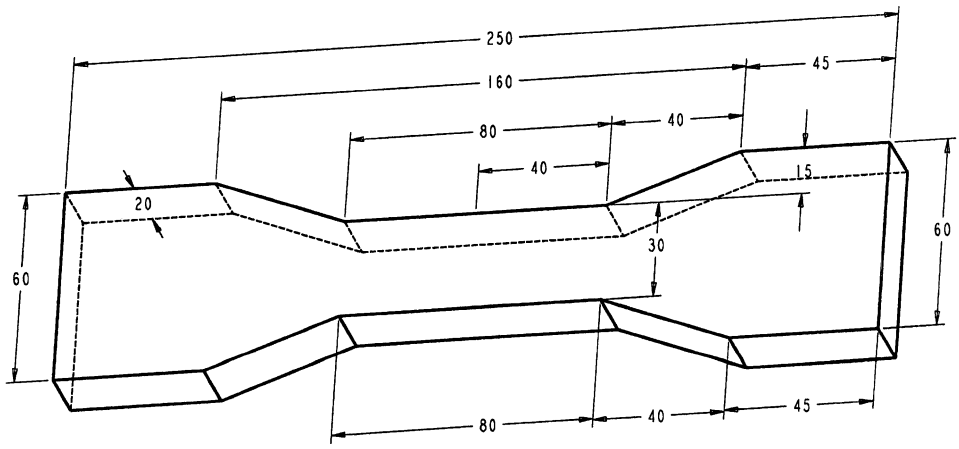

Fig. 2. Specimen configuration. Dimensions are in millimeters.

centers of the opposite sides at the narrow part of the dog-bone shaped specimen. Simultaneously with mechanical testing the DC electrical resistance was measured using the four-probe method. The longitudinal resistance was measured along the stress axis. The electrical contacts, made with silver paint and applied along the whole perimeter of the four parallel planes perpendicular to the stress axis, symmetrically located in the narrow part of the dog-bone shape. The inner two contacts (70 mm apart) were used for voltage measurement, while the outer two contacts (80 mm apart) were used for passing current. The longitudinal and transverse strains and the longitudinal resistance were simultaneously measured for each specimen. A Keithley 2001 multimeter was used.

The resistivity was measured using the resistance and the dimensions. Both longitudinal and transverse strains were obtained, except for the case of longitudinal resistivity measurement during uniaxial compression, when the longitudinal strain measurement was made. Neglecting the transverse strain actually affected the resistivity value slightly. The fractional change in resistance was essentially equal to the fractional change in resistivity.

Due to the voltage present during electrical resistance measurement, electric polarization occurs continuously as the resistance measurement is made. The polarization results in an increase in the measured resistance [34]. The polarization-induced resistance increase was separately measured as a function of the time of resistance measurement in the absence of stress. It was subtracted from the measured resistance change obtained during cyclic loading in order to correct for the effect of polarization.

3. Results and discussion

3.1. Effect of silica fume

Figs. 3 and 4 show the variation of the fractional change in longitudinal resistivity with cycle number during initial cyclic compression of plain mortar and silica fume mortar,

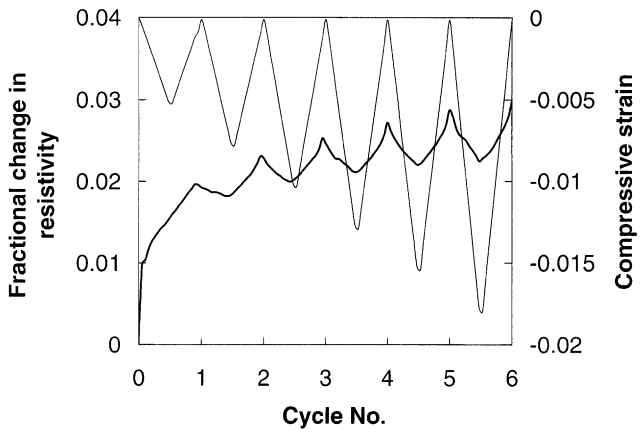

Fig. 3. Variation of the fractional change in resistivity with cycle number (thick curve) and of the compressive strain with cycle number (thin curve) during repeated compressive loading at increasing stress amplitudes within the elastic regime for plain mortar.

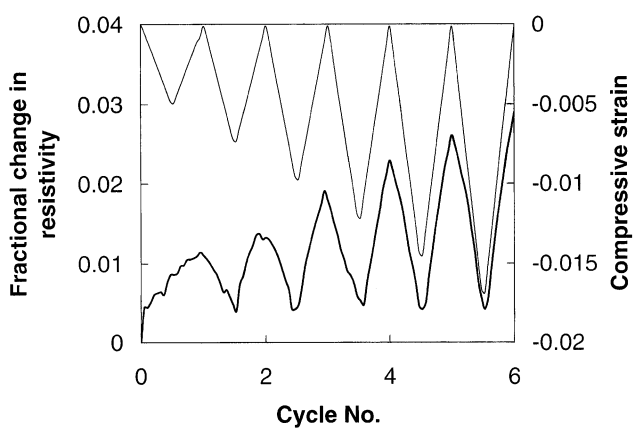

Fig. 4. Variation of the fractional change in resistivity with cycle number (thick curve) and of the compressive strain with cycle number (thin curve) during repeated compressive loading at increasing stress amplitudes within the elastic regime for silica fume mortar.

respectively. The stress amplitude used increased cycle by cycle. For both mortars, the resistivity increased abruptly during the first loading (due to defect generation [1]) and increased further during the first unloading (due to defect aggravation [1]). Moreover, the resistivity decreased during subsequent loading (due to defect healing [1]) and increased during subsequent unloading (due to defect aggravation [1]); the effect associated with defect healing was much larger for silica fume mortar than for plain mortar. In addition, this effect intensified as stress cycling at increasing stress amplitudes progressed for both mortars, probably due to the increase in the extent of minor damage. The increase in damage extent was also indicated by the resistivity baseline increasing gradually cycle by cycle. In spite of the increase in stress amplitude cycle by cycle, defect healing dominated over defect generation during loading in all cycles other than the first cycle.

Comparison of Figs. 3 and 4 showed that silica fume contributed significantly to the defect dynamics. The associated defects were presumably at the interface between silica fume and cement, even though this interface was diffuse due to the pozzolanic nature of silica fume. The defects at this interface were presumably smaller than those at the sand–cement interface, due to the small particle size of silica fume compared to sand. However, this interface was large in total area due to the small size of silica fume.

3.2. Effect of sand

Comparison of plain cement paste behavior [1] and plain mortar behavior (this work) showed that the behavior was similar, except that the defect healing (i.e., the resistivity decrease upon loading other than the first loading) was much more significant in the mortar case. This means that the sand–cement interface in the mortar contributed significantly to the defect dynamics, particularly in relation to defect healing. This is probably due to the large size of the defects associated with this interface, compared to those associated with the interface between silica fume and cement.

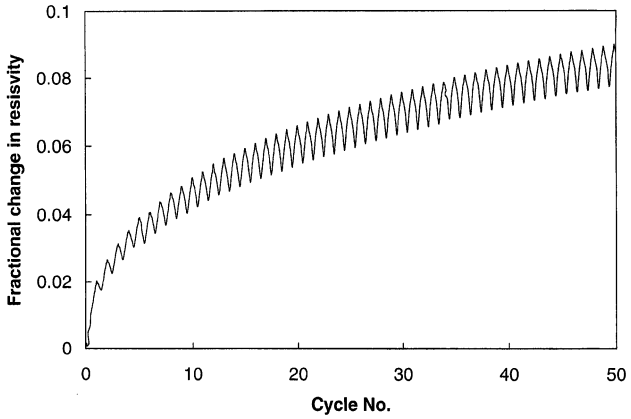

Fig. 5. Fractional change in longitudinal resistivity versus compressive stress cycle number for plain mortar in Cycles 1–50.

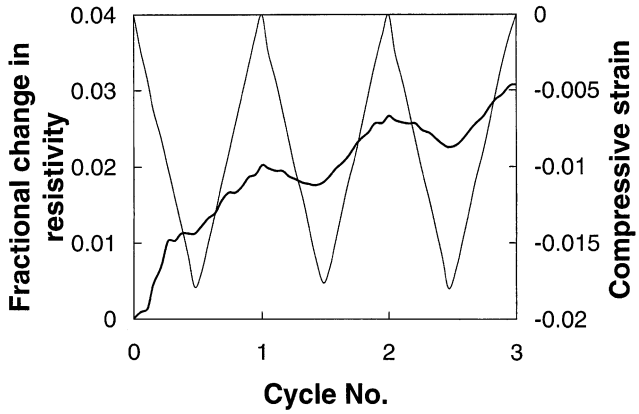

Fig. 6. Fractional change in longitudinal resistivity (solid curve) and longitudinal strain (dashed curve), both versus compressive stress cycle number for plain mortar in Cycles 1–3.

3.3. Uniaxial compression

Figs. 5–7 show the fractional change in longitudinal resistivity versus cycle number during cyclic compression. The stress amplitude was fixed at 34.5 MPa. Except for the first cycle, the resistivity decreased with increasing strain in each cycle and then increased upon subsequent unloading in the same cycle. This effect is attributed to defect healing (reversible) under the compressive stress. As cycling progressed, the baseline resistivity continuously increased, such that the increase was quite abrupt in the first three cycles (Fig. 5) and that subsequent baseline increase was more gradual. This irreversible effect is probably due to minor damage, i.e., damage accumulation as cycling progressed. (Identification of the type of damage is beyond the scope of this paper.) The incremental increase in damage diminished as cycling progressed. This means that the damage is not due to fatigue. In addition, as cycling progressed, the amplitude of resistivity decrease within a cycle gradually and continuously increased (Fig. 5). This is probably because the

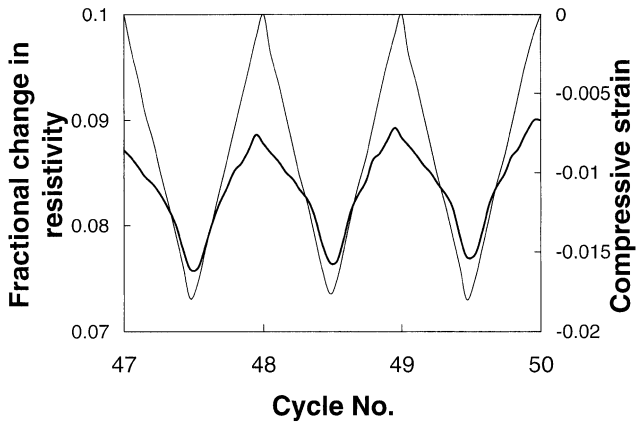

Fig. 7. Fractional change in longitudinal resistivity (solid curve) and longitudinal strain (dashed curve), both versus compressive stress cycle number for plain mortar in Cycles 48–50.

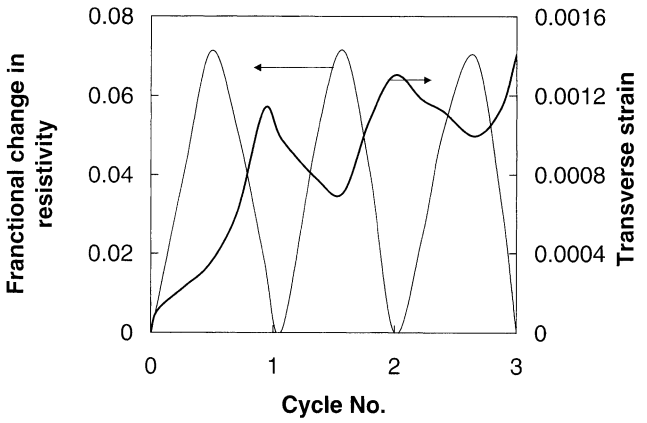

Fig. 8. Variation of the fractional change in transverse resistivity (thick curve) with time and of the transverse strain (thin curve) with time during dynamic compressive loading of plain mortar in Cycles 1–3 at a constant stress amplitude of 13.90 MPa.

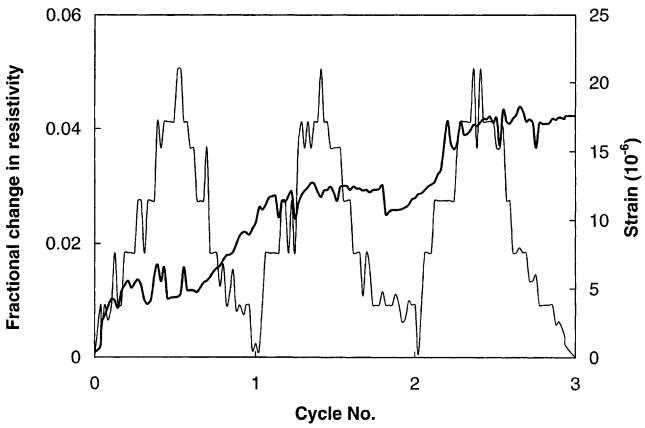

Fig. 10. Variation of the fractional change in longitudinal electrical resistivity with cycle number (thick curve) and of the strain with cycle number (thin curve) during cyclic uniaxial tensile loading at a constant stress amplitude of 1.48 MPa for plain mortar in Cycles 1–3.

cumulative damage (as indicated by the baseline resistivity) increased and resulted in a greater degree of defect healing upon compression (hence, more decrease in resistivity within a cycle). Hence, the reversible effect of defect healing is affected by the irreversible accumulation of damage.

Fig. 8 shows the fractional change in transverse resistivity as well as the transverse strain (positive due to the Poisson effect) during repeated compressive loading of plain mortar at a constant compressive stress amplitude of 13.9 MPa. The strain varied linearly with the stress and returned to zero at the end of each cycle of loading. During the first loading and the first unloading, the resistivity increased due to defect generation and defect aggravation respectively, as also shown by the longitudinal resistivity variation (Fig. 8). During the second loading, the resistivity decreased (due to defect healing). During the second unloading, the resistivity increased, due to defect aggravation. During the third loading, the resistivity decreased due to defect healing. During the third unloading, the resistivity increased, due to defect aggravation. The resistivity baseline shifted upward as cycling progressed, as shown in Fig. 9.

The variations of the resistivity in the longitudinal and transverse directions upon repeated loading are consistent in showing defect generation (which dominates during the first loading), defect healing (which dominates during subsequent loading) and defect aggravation (which dominates during subsequent unloading). The defect aggravation during unloading follows the defect healing during loading, indicating the reversible (not permanent) nature of the healing, which is induced by compressive stress. The defect aggravation during unloading also follows the defect generation during loading.

In spite of the Poisson effect, similar behavior was observed in the longitudinal and transverse resistivities. This means that the defects mentioned above are essentially nondirectional and that the resistivity variations are real.

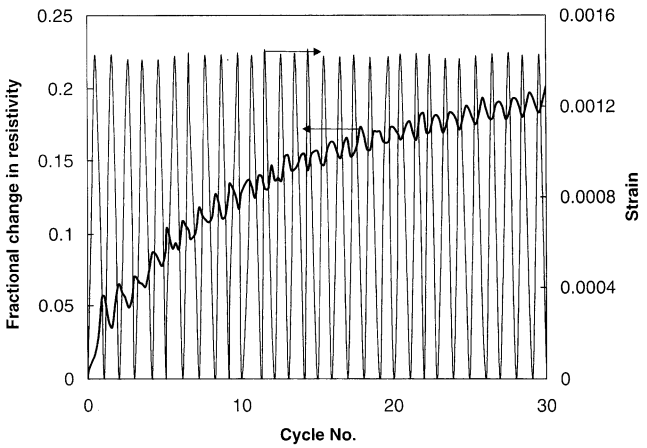

Fig. 9. Variation of the fractional change in transverse resistivity (thick curve) with time and of the transverse strain (thin curve) with time during dynamic compressive loading of plain mortar in Cycles 1–30 at a constant stress amplitude of 13.90 MPa.

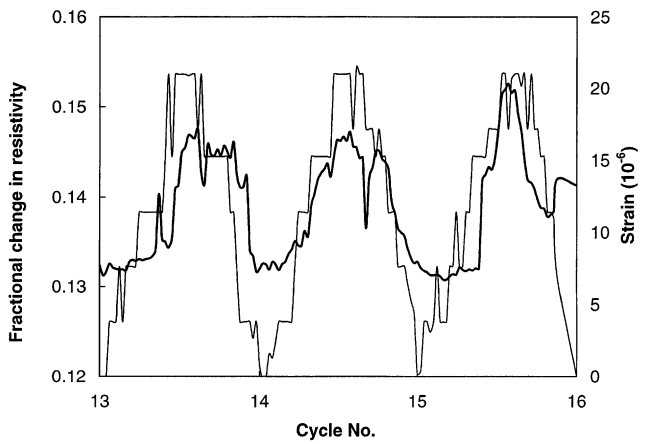

Fig. 11. Variation of the fractional change in longitudinal electrical resistivity with cycle number (thick curve) and of the strain with cycle number (thin curve) during cyclic uniaxial tensile loading at a constant stress amplitude of 1.48 MPa for plain mortar in Cycles 14–16.

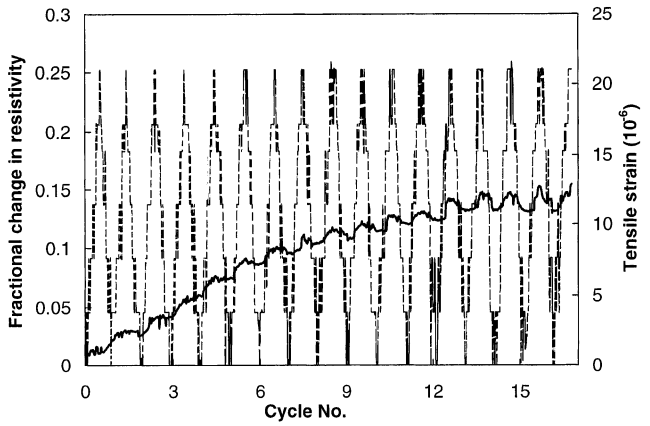

Fig. 12. Variation of the fractional change in longitudinal electrical resistivity with cycle no. (solid curve) and of the strain with cycle no. (dashed curve) during cyclic uniaxial tensile loading at a constant stress amplitude of 1.48 MPa for plain mortar in Cycles 1–16.

3.4. Uniaxial tension

Fig. 10 shows the fractional change in longitudinal resistivity during uniaxial tension of plain mortar at a constant stress amplitude of 1.48 MPa in the elastic regime. The longitudinal resistivity and strain increased reversibly upon tension, due to defect generation and aggravation upon loading and partial defect healing upon unloading. The change of resistivity within a cycle became more pronounced as cycling progressed, as shown by comparing Fig. 11 (Cycles 14–16) with Fig. 10 (Cycles 1–3). This trend is attributed to the increase in the cumulative amount of defects as cycling progressed. In addition, the resistivity baseline gradually shifted upward as cycling progressed, as shown in Fig. 12.

3.5. Comparison of uniaxial compression and uniaxial tension

Comparison of Figs. 8 and 10 showed that the longitudinal resistivity under uniaxial tension (Fig. 10) increased with the tensile strain, whereas the transverse resistivity under uniaxial compression (Fig. 8) decreased with the transverse tensile strain. Thus, the strain in the resistivity direction does not govern how the resistivity changes with strain. Rather, the mode of stress application (uniaxial tension vs. uniaxial compression) is the governing factor. This means that the resistivity in any direction relative to the stress axis can be used to indicate the occurrence of uniaxial compression or tension. A decrease in resistivity indicates the occurrence of uniaxial compression, except for the first compressive cycle; an increase in resistivity indicates the occurrence of uniaxial tension.

That the mode of stress application rather than the strain in the resistivity direction governs how the resistivity varies with strain has been previously reported for carbon fiber cement paste, which was similarly studied under uniaxial compression [35] and under uniaxial tension [36], though the resistivity variation is less noisy when the fibers are present.

The upward shift of the resistivity baseline as cycling progressed was observed under uniaxial tension (Fig. 12) and under uniaxial compression (Figs. 5 and 9). The shift was observed for the longitudinal resistivity (Fig. 5) as well as the transverse resistivity (Fig. 9). This irreversible phenomenon is probably due to minor damage, as the effect of polarization has been removed by subtraction.

4. Conclusion

The defects associated with both the interface between sand and cement and that between silica fume and cement respond in a dynamic fashion to repeated loading, thus contributing significantly to the defect dynamics of cement mortar, particularly in relation to defect healing. The defect dynamics involve defect generation, defect healing and defect aggravation. Defect generation dominates in the first compressive loading and in tensile loading in any loading cycle. Defect healing dominates in all subsequent compressive loading and in tensile unloading in any cycle. Defect aggravation dominates during compressive unloading in any cycle and also occurs during tensile loading in any cycle. The defect dynamics give similar effects to the longitudinal and transverse resistivities. Upon uniaxial compression, the resistivity decreases (except for the first cycle); upon uniaxial tension, the resistivity increases.

Acknowledgments

This work was supported by National Science Foundation, USA.

References

[1] S. Wen, D.D.L. Chung, Defect dynamics of cement paste under repeated compression, studied by electrical resistivity measurement, Cem. Concr. Res. 31 (10) (2001) 1515–1518.
[2] S. Wen, D.D.L. Chung, Damage monitoring of cement paste by electrical resistance measurement, Cem. Concr. Res. 30 (12) (2000) 1979–1982.
[3] M.J. Schmidt, C.A. Ross, Shear strength of concrete under dynamic loads, ASME, Pressure Vessels Piping Div. 394 (1999) 121–127.
[4] N. Burlion, F. Gatuingt, G. Pijaudier-Cabot, L. Daudeville, Compaction and tensile damage in concrete: Constitutive modelling and application to dynamics, Comput. Methods Appl. Mech. Eng. 183 (3) (2000) 291–308.
[5] A.H. Al-Gadhib, M.H. Baluch, A. Shaalan, A.R. Khan, Damage model for monotonic and fatigue response of high strength concrete, Int. J. Damage Mech. 9 (1) (2000) 57–78.
[6] W. Sun, Y.M. Zhang, H.D. Yan, R. Mu, A. Yan, Damage and its restraint of concrete with different strength grades under double damage factors, Cem. Concr. Compos. 21 (5–6) (1999) 439–442.

[7] F. Stangenberg, W.B. Kraetzig, Y.S. Petryna, M. Roik, Reliability assessment of reinforced concrete structures with respect to material degradation, Structures Congress — Proceedings, pp. 154–157.
[8] E.N. Landis, D.T. Keane, X-ray microtomography for fracture studies in cement-based materials, Proc. SPIE-Int. Soc. Opt. Eng. 3772 (1999) 105–113.
[9] S. Yuyama, Z.-W. Li, Y. Ito, M. Arazoe, Quantitative analysis of fracture process in RC column foundation by moment tensor analysis of acoustic emission, Constr. Building Mater. 13 (1) (1999) 87–97.
[10] E.N. Landis, Micro–macro fracture relationships and acoustic emissions in concrete, Constr. Building Mater. 13 (1) (1999) 65–72.
[11] M.L. Wang, Z.L. Chen, Simulation of the failure mechanisms of quasi-brittle materials, Constr. Building Mater. 13 (1) (1999) 49–55.
[12] A. Ghobarah, A. Biddah, Dynamic analysis of reinforced concrete frames including joint shear deformation, Eng. Struct. 21 (11) (1999) 971–987.
[13] M.W. Lin, A.O. Abatan, W.-M. Zhang, Crack damage detection of concrete structures using distributed electrical time domain reflectometry (ETDR) sensors, Proc. SPIE-Int. Soc. Opt. Eng. 3671 (1999) 297–304.
[14] D. Boudon-Cussac, F. Hild, G. Pijaudier-Cabot, Tensile damage in concrete: Analysis of experimental technique, J. Eng. Mech.—ASCE 125 (8) (1999) 906–913.
[15] J. Zelic, R. Krstulovic, E. Tkalcec, P. Krolo, Properties of Portland cement–limestone–silica fume mortars, Cem. Concr. Res. 20 (1) (2000) 145–152.
[16] Anonymous, High performance cement: A solution for next millennium, Mater. Technol. 14 (4) (1999) 191–193.
[17] M. Hisada, S. Nagataki, N. Otsuki, Evaluation of mineral admixtures on the viewpoint of chloride ion migration through mortar, Cem. Concr. Compos. 21 (5–6) (1999) 443–448.
[18] M.G. Alexander, B.J. Magee, Durability performance of concrete containing condensed silica fume, Cem. Concr. Res. 29 (6) (1999) 917–922.
[19] J. Zelic, R. Krstulovic, E. Tkalcec, P. Krolo, Durability of the hydrated limestone–silica fume Portland cement mortars under sulphate attack, Cem. Concr. Res. 29 (6) (1999) 819–826.
[20] R.S. Santos, F.A. Rodrigues, N. Segre, I. Joekes, Macro-defect free cements: Influence of poly(vinyl alcohol), cement type, and silica fume, Cem. Concr. Res. 29 (5) (1999) 747–751.
[21] M.D.A. Thomas, M.H. Shehata, S.G. Shashiprakash, D.S. Hopkins, K. Cail, Use of ternary cementitious systems containing silica fume and fly ash in concrete, Cem. Concr. Res. 29 (8) (1999) 1207–1214.
[22] Z. Liu, J.J. Beaudoin, Assessment of the relative permeability of cement systems using AC impedance techniques, Cem. Concr. Res. 29 (7) (1999) 1085–1090.
[23] B.S. Hamad, M.F. Machaka, Effect of transverse reinforcement on bond strength of reinforcing bars in silica fume concrete, Mater. Struct. 32 (220) (1999) 468–476.
[24] B. Ma, J. Li, J. Peng, Influence of mineral admixtures on mechanical properties of high-performance concrete, J. Wuhan Univ. Technol., Mater. Sci. Ed. 14 (2) (1999) 1–7.
[25] C.S. Poon, L. Lam, Y.L. Wong, Effects of fly ash and silica fume on interfacial porosity of concrete, J. Mater. Civil Eng. 11 (3) (1999) 197–205.
[26] H.A. Toutanji, Z. Bayasi, Effect of curing procedures on properties of silica fume concrete, Cem. Concr. Res. 29 (4) (1999) 497–501.
[27] F. Collins, J.G. Sanjayan, Effects of ultra-fine materials on workability and strength of concrete containing alkali-activated slag as the binder, Cem. Concr. Res. 29 (3) (1999) 459–462.
[28] S.B. Park, E.S. Yoon, B.I. Lee, Effects of processing and materials variations on mechanical properties of lightweight cement composites, Cem. Concr. Res. 29 (2) (1999) 193–200.
[29] H. Yan, W. Sun, H. Chen, Effect of silica fume and steel fiber on the dynamic mechanical performance of high-strength concrete, Cem. Concr. Res. 29 (3) (1999) 423–426.
[30] H.A. Toutanji, L. Liu, T. El-Korchi, Role of silica fume in the direct tensile strength of cement-based materials, Mater. Struct. 32 (217) (1999) 203–209.
[31] V.G. Papadakis, Experimental investigation and theoretical modeling of silica fume activity in concrete, Cem. Concr. Res. 29 (1) (1999) 79–86.
[32] V. Matte, M. Moranville, Durability of reactive powder composites: Influence of silica fume on the leaching properties of very low water/binder pastes, Cem. Concr. Compos. 21 (1) (1999) 1–9.
[33] H. El-Didamony, A. Amer, M. Heikal, Improvement of silica fume blended cements by using superplasticizer, Ceram.-Silik. 42 (4) (1998) 171–176.
[34] S. Wen, D.D.L. Chung, Electric polarization in carbon fiber reinforced cement, Cem. Concr. Res. 31 (2) (2001) 141–147.
[35] S. Wen, D.D.L. Chung, Uniaxial compression in carbon fiber reinforced cement sensed by electrical resistivity measurement in longitudinal and transverse directions, Cem. Concr. Res. 31 (2) (2001) 297–301.
[36] S. Wen, D.D.L. Chung, Uniaxial tension in carbon fiber reinforced cement, sensed by electrical resistivity measurement in longitudinal and transverse directions, Cem. Concr. Res. 30 (8) (2000) 1289–1294.